Cold Regions Science and Technology, 20 (1992) 119–139
Elsevier Science Publishers B.V., Amsterdam

Stress measurements in drifting pack ice

Walter B. Tucker III and Donald K. Perovich
U.S. Army Cold Regions Research and Engineering Laboratory, 72 Lyme Road, Hanover, NH 03755, USA

(Received 7 December 1990; after revision accepted 3 April 1991)

ABSTRACT

Tucker, W.B. III and Perovich, D.K., 1992. Stress measurements in drifting pack ice. *Cold Reg. Sci. Technol.*, 20: 119–139.

Accurate measurements of *in-situ* pack ice forces are necessary to improve ice forecasting models and to estimate loads on offshore structures. Two months of *in-situ* ice stress measurements were obtained in the pack ice of the eastern Arctic during the fall of 1988. Sensors were placed to examine both the horizontal and vertical distributions of ice stresses in multiyear ice. Stresses in the multiyear ice 200 m from the edge of the floe reached 150 kPa during extreme deformation events. Within a few meters of the edge and in adjacent first-year ice, they exceeded 350 kPa on several occasions (400 kPa in one instance) during local ice failure events. Thermally induced stresses at shallow depths in the multiyear ice were caused by rapid temperature changes and could be nearly as large as stresses observed during deformation. The vertical distribution of stresses varied with the type of deformation event, but the largest values were always observed in the upper half of the ice sheet. Stresses due to deformation were rapidly attenuated away from the edge of the floe. Near the edge, however, recorded stresses agreed well with those observed in the adjacent first-year ice. These two locations also experienced twice daily oscillations of about 50 kPa which are apparently tidal or inertially induced.

Introduction

Wind and current forces acting on a sea ice cover impart stresses into the ice which are transmitted through the cover to near or distant locations. The accompanying movement and deformation of the ice cover dissipates this energy. The ice forces associated with deformation, primarily ridge building, are equivalent to the maximum stresses that can be sustained and transmitted by the ice pack, thus they essentially represent the strength of the ice (Rothrock, 1975; Hibler, 1980). At present, we lack the clear understanding of the forces involved in deformation that is needed to substantially improve ice dynamics models and to better estimate loads on offshore structures. Although the temporal and spatial resolution of ice forecasting models can be increased, model results will not improve significantly until a more realistic accounting of the mechanical processes at smaller scales is included. For offshore Arctic operations, the forces involved in local ridge building will dominate the loaded placed on man-made structures in certain situations (Croasdale et al., 1988), thus knowing the force magnitudes would greatly enhance the determination of design loads.

In reviewing previously published investigations of ridge building forces, Vivatrat and Kreider (1981), Croasdale (1984) and Croasdale et al. (1988) found that estimates of the forces varied by over an order of magnitude. While some of this difference is due to the presumed failure occurring over large wide or small narrow fronts, there remains considerable variation in the estimates. Until recently, none of the existing ridge building force estimates had been obtained from actual full-scale field measurements, primarily because of the difficulty involved in obtaining accurate measurements. Recent investigations (Croasdale et al., 1988;

Coon et al., 1989; Comfort and Ritch, 1990), however, have attempted to monitor pack ice forces using a variety of instruments designed to measure *in-situ* ice stresses.

The petroleum industry can be credited with much of the work to date on the measurement and prediction of ice forces and certainly with the development of instrumentation capable of making such measurements. The primary interest in previous industry studies was in the measurement of local ice forces on offshore structures (e.g., Graham et al., 1983; Hawkins et al., 1983). In the pursuit of obtaining optimal design loads for structures, a variety of sensors were developed for the measurement of *in-situ* ice stresses. Many of these sensors have been used in recent field programs. Croasdale et al. (1988) used strain-gauged metal buttons and hydraulic flatjacks which were placed in the center of a large multiyear floe in the southern Beaufort Sea. A 22 kPa stress change, observed during a small ridging event, was the largest compressive stress measured. Coon et al. (1989) used hydraulic flatjacks in the eastern Arctic, and reported an *in-situ* stress of about 35 kPa during a ridging event. Comfort and Ritch (1990) used two types of flatjacks and strain-gauged metal buttons, again on a large floe in the Beaufort Sea. They reported maximum stresses of 190 kPa during one ridging event, considerably larger than those reported in the other studies. Comfort and Ritch (1990) also investigated the vertical and horizontal distribution of stresses in the ice.

This paper discusses a stress measurement program in which biaxial vibrating wire stress sensors were used to monitor pack ice stresses on the drift phase of the Coordinated Eastern Arctic Experiment (CEAREX). On the drift phase, the Norwegian charter vessel Polarbjorn was moored to a multiyear floe and allowed to drift with the pack while the behavior of the ice, ocean and atmosphere were monitored. After initial emplacement in the ice with the assistance of the U.S. Coast Guard Icebreaker Northwind, the Polarbjorn drifted from 82°40'N, 32°26'E to 80°10'N, 31°13'E from September 18 to November 25, 1988 (Fig. 1). During this period, the meteorological program consisted of continuous measurements of standard surface phenomena, turbulent heat and momentum statistics and upper air winds, temperatures and humidities. Oceanographic measurements consisted of CTD casts, boundary layer turbulence and continuous monitoring of currents. Ice measurements included ice stress, local ice deformation and acceleration, far field deformation and drift, ice growth and ablation, physical and mechanical properties. Ambient noise in the ocean was monitored using hydrophones placed beneath the ice.

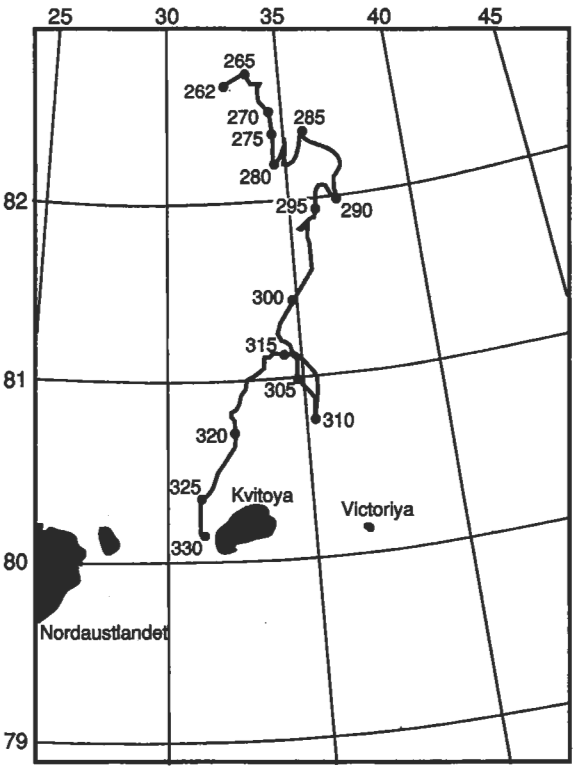

Fig. 1. Drift track of the Polarbjorn from day 262 (September 18) to day 330 (November 25).

This joint experiment provided an ideal setting for measuring ice stresses because they could be correlated with other environmental parameters. The primary objective of the stress program was to monitor pack ice geophysical stresses in the eastern Arctic for the two month drift period. It was anticipated that the ice would drift around the north coast of Spitsbergen and into the Fram Strait. We believed that large ice stresses would be experienced as the ice was compressed against Spitsbergen as it entered Fram Strait. Instead, the local pack ice drifted to the east of Spitsbergen and entered the

Barents Sea. Nonetheless, large stresses were observed during deformation of the ice as it compressed and sheared against Kvitoya Island. Another major objective was to investigate vertical and horizontal variations in stress on the floe. This was facilitated by the use of the vibrating wire sensors which are easily installed at any depth. A final objective was to compare stresses in thin first-year ice to those in adjacent multiyear ice.

High-quality pack ice stress data was obtained during the CEAREX drift program. Preliminary results have been reported by Tucker et al. (1991) where the measured stresses from one site were contrasted to the local strain field. Little correlation between local stress and strain was found in that investigation, emphasizing the complexity of ice interaction during deformation. The investigation described here presents the two months of measurements of ice stresses and our interpretation of the results. We were fortunate to monitor stresses during the complete disintegration of floes in the area during the large deformation at the end of the experiment. *In-situ* ice stresses were measured at different vertical levels and different horizontal locations. In many cases we have been able to attribute different geophysical causal mechanisms to the observed stresses.

Field measurements

Stress sensors

The stress measurements described in this investigation were obtained with biaxial vibrating wire stress sensors similar to those described by Cox and Johnson (1983). These instruments were chosen because of their relative ease of installation and maintenance, the extensive calibrations that had been previously performed (Cox and Johnson, 1983), and their success in earlier field programs (Johnson et al., 1985). The sensor consists of a stiff steel cylinder which is 0.25 m long, 57 mm in diameter and has a wall thickness of 16 mm. The gauge is much stiffer than the ice, having a modulus of about 200 GPa, thus should not be affected by spatial variations or temporal changes of the ice modulus. Six tensioned wires are set at 30° intervals across the inside diameter of the gauge. Only three wires are necessary for the determination of principal stress components; the remaining wires are for redundancy.

The principal stress components in the plane of the wires (the horizontal plane of the ice) are obtained from measurements of the radial deformation of the cylinder wall. The deformation of the gauge in the three wire directions is determined by the resonant frequency of each wire after it has been plucked by a magnet/coil assembly. Knowing the geometry and material properties of the sensor and ice, the principal components (σ_1,σ_2) and direction (θ) of stress are calculated directly from the radial deformation of the gauge.

Cox and Johnson (1983) conducted extensive tests in which both fresh and saline ice samples containing the stress sensors were loaded in a variety of configurations. These tests indicated that the gauge accuracy was better than 15% and the resolution exceeded 20 kPa. These elaborate tests proved convincingly that both the gauges and the theory for determining ice stresses were adequate for *in-situ* measurements. Recently, the resolution of the gauges has been improved to an estimated 5 kPa through the use of a superior data-logging system.

Prior to use in our field program, each sensor was subjected to pressure and temperature calibrations. The pressure calibrations consisted of determining the frequency of each vibrating wire under hydrostatic loads ranging from 0 to 1000 kPa. These tests provide the constants necessary to compute the radial deformations. We also attempted to conduct temperature calibrations on the sensors. The calibrations were unsuccessful, however, because rapidly varying temperatures induce a stress in the gauge by causing a large temperature gradient through the sensor wall. The cycling of the glycol bath in which the temperature calibrations were conducted was sufficient to induce these stresses. At the conclusion of the field experiment, however, temperature calibrations were conducted on several of the recovered sensors by placing the sensors in a precision-controlled environmental chamber. These tests verified that the temperature sensitivities of the gauges were very small, a result previously found by Cox and Johnson (1983).

There are serious concerns regarding the mea-

surement of *in-situ* ice stresses with small sensors. Some of these issues have been addressed by Comfort and Ritch (1990) and Croasdale et al. (1988). Among the foremost is the question of the relationship between the stress measured by the sensor and the actual *in-situ* ice stress, the inclusion factor. The inclusion factor has been well established for these sensors by the extensive in-ice calibrations of Cox and Johnson (1983) and is accounted for in the stress reduction procedure. Other concerns regarding the sensor performance included the effects that freeze-in stresses would have on the sensors and whether or not the sensors would experience long-term drift. We experienced both problems and our resolution is described in the Results section. Another major concern is the relationship between the very local stresses measured at the sensor and the actual distribution of stresses in the floe or the mean ridge-building forces in the local pack ice. This is of particular concern when one considers the variability of thicknesses and mechanical properties of multiyear floes and the likelihood of having nonsimultaneous failure during deformation. Recent modeling indicates that average pack ice stresses can best be determined by measuring the stress at the center of the multiyear floe (Frederking and Evgin, 1990). However, the vertical and horizontal variations of stresses is an area that has only begun to be addressed by modeling efforts. We investigated the spatial variability of stress by placing the sensors both vertically through the thickness of the floe and in different horizontal locations at the same depths.

Field installation

The Polarbjorn was moored to a multiyear floe on September 16, 1988 at 82°40'N, 32°26'E. Four stress sensor sites were established over the next two weeks, on each of two adjacent multiyear floes. Because of sensor and data logger difficulties, data from two of the sites were unreliable and are not presented. Figure 2 shows the configuration of the stress sensor sites on the two floes. At site 1, on floe Alpha, three sensors were installed at vertical levels near the top, mid-depth and bottom of the ice sheet. At site 2, which was located on the edge of the multiyear floe Beta adjacent to a freezing lead, one sensor was placed in the first-year ice while the remaining two were located at shallow depths in the multiyear ice.

The sensors were installed in holes approximately 0.1 m in diameter made with a standard ice coring auger. Each sensor was attached to a length of PVC pipe which was suspended to the proper depth from the surface by a cross bar through the PVC extension. Once the sensor was placed in the hole at the proper depth, and leveled in the horizontal plane, the hole was filled with fresh water. Depending upon the air and ice temperature, the hole was usually completely frozen within a day or two. Stresses associated with the freeze-in were as large as 300 kPa, and took several days to attenuate.

Site 1 was located on 1.60 m thick multiyear ice about 200 m from the edge of the floe. Sensors were installed at depths of 0.25, 0.70 and 1.20 m. At site 2, one sensor was located in the first-year ice at a depth of 0.20 m. The thickness of this frozen lead increased from 0.38 to 0.54 m during the stress-monitoring period. The sensor was located about 7.0 m from the edge of the multiyear floe in the thin ice which was about 200 m wide. The two remaining sensors were positioned at 0.25 m depths in 2.0 m thick multiyear ice, at distances of 2 and 15 m from the edge of the floe. The three sensors were configured in a straight line normal to the edge of the floe and the frozen lead.

Data from each site was recorded on Campbell Scientific, Inc. data loggers. The sensors were sampled and recorded at two minute intervals, and the period (frequency) of each wire in each sensor was stored. The data loggers cached data in memory modules which required replacement with empty modules at 5 to 7 day intervals. Normally, no interruption in sampling occurred during this exchange, though there were occasional breaks in the data if the memory modules were filled to capacity.

Several ancillary ice measurements were made to complement the stress measurements. Thermistor strings were placed through the thickness of the ice so that the temperature of the ice sheet could be continuously monitored. The thermistors were sampled at hourly intervals by the same data loggers that recorded the stress measurements. Manually operated ice ablation gauges were also located at each site and the ice thickness changes were monitored at 5 day intervals. Small-scale ice properties

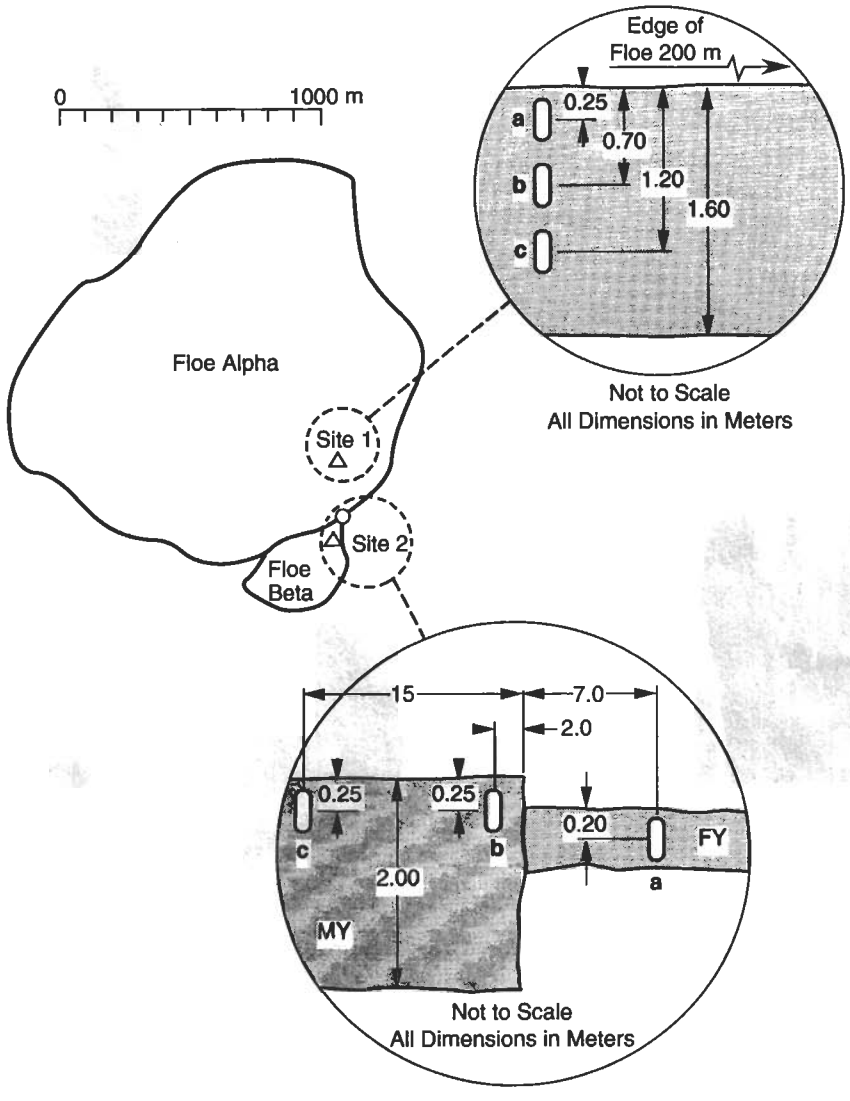

Fig. 2. Schematic of Alpha and Beta floes illustrating the locations of the stress sensor sites. Inserts show configuration of sensors at each site.

at each site were determined by coring. Vertical profiles of salinity, temperature, density and ice crystallography were determined from the core. The ice properties schematic from site 1 on day 309 is shown in Fig. 3. The figure indicates that the ice was composed of columnar congelation crystals. Horizontal thin sections show very little alignment of crystal *c*-axes. The temperature increased almost linearly from $-19°C$ at the snow–ice interface to $-2.0°C$ at the bottom. Salinity was also very low at the surface and slowly increased with depth. Using the equations of Cox and Weeks (1983), the brine and air volumes of the ice were determined from the temperature, salinity and density profiles. These values allowed the effective modulus to be calculated from the empirical relationships developed by Vaudrey (1977) and modified by Tucker et al. (1989) to account for the increased air volumes in multiyear ice.

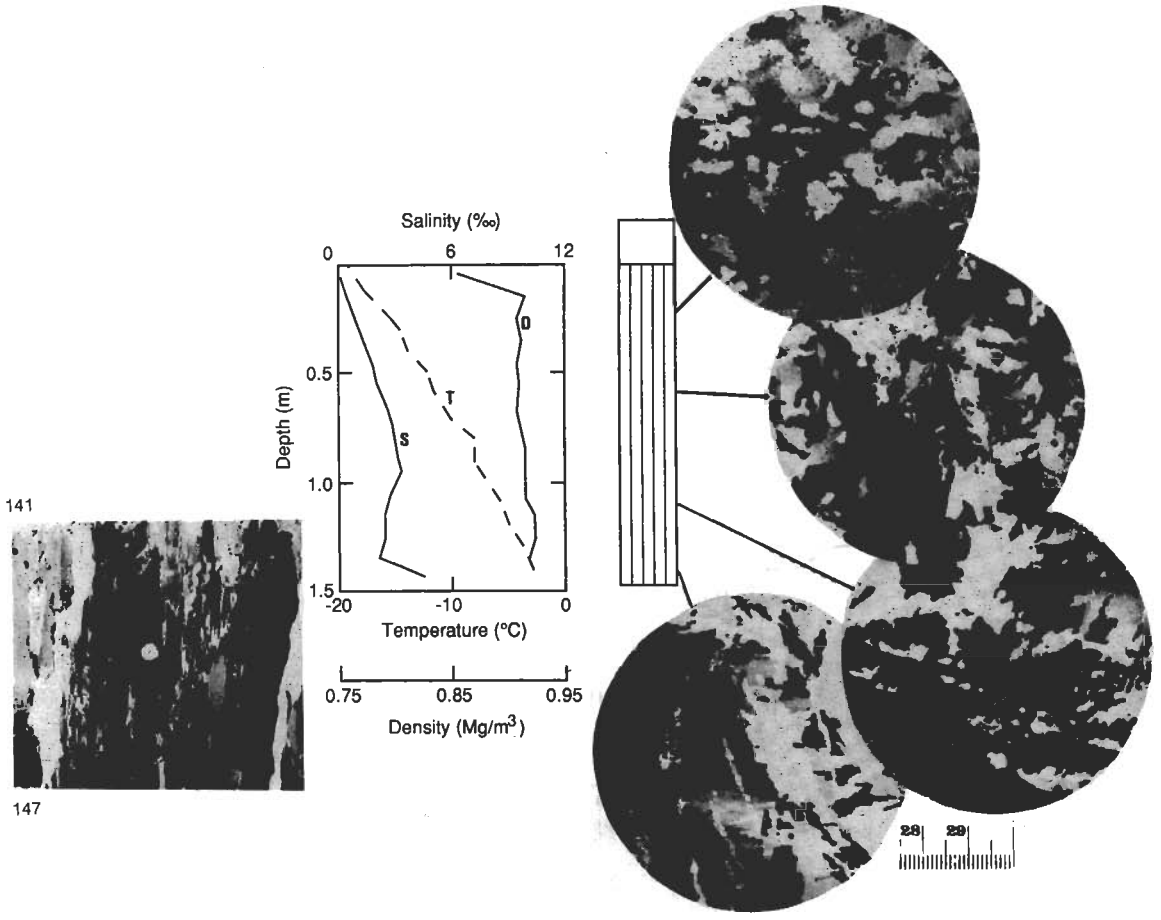

Fig. 3. Ice properties from site 1. Profiles include salinity (S), temperature (T), and density (D). Structural schematic indicates congelation texture.

Results and discussion

Residual stresses

Freeze-in stresses were observed for 2 to 4 days after the sensors were placed in the ice. The freeze-in stress was normally characterized by an initial compressive stress of 50 to 300 kPa which gradually decreased within the 2 to 4 day period. On most sensors, however, the stresses did not return to the zero stress levels determined from the calibrations. Residual tensile or compressive stresses of 10 to 40 kPa were indicated by most sensors. Comfort and Ritch (1989) found similar residual stresses in their measurements in the Beaufort Sea. It is possible that these stresses were ambient ice stresses. However, *in-situ* stresses due to in-plane forces should have dissipated during periods when open water was observed locally. It is possible that they are caused by local effects such as isostatic inequilibrium. We suspect, however, that they are the result of local sensor/ice interaction resulting from freeze-in, but a more precise determination of the cause of the residual stresses remains elusive. In addition to the residual stresses, a minor amount of long-term drift occurred in the stress records of some of the sensors. The maximum drift magnitude was about 40 kPa over the 60 day period. The drift is probably due to changes in the length of the vibrating wires caused by long-term temperature effects of extended use. Not every sensor experienced the long-term drift, but all sensors except the sensor installed

in first-year ice showed some evidence of residual stress. It is likely that the lower ice modulus and the more ductile behavior allows the first-year ice to rapidly dissipate residual stresses.

The residual stresses and the long-term drift were removed from the records of each sensor. Two short periods near the beginning and end of the experiment were designated as "zero stress" times. A linear fit to the stresses occurring at these times was removed from the stress record of each sensor. The two periods were selected based on the criteria that they were stress minima on all sensors, thermal fluctuations in the ice were small, the wind velocities were small, the strain monitoring equipment indicated no active convergence, and finally, visual observations indicated open water in the area. While we cannot be absolutely certain that the stresses presented have been reduced to their precise ambient levels, we are confident that the variations in stress are accurate. It is the stress changes associated with individual "events" that are of most interest.

Site 1 time series

The longest time series of continuous stress measurements was recorded at site 1 for the sensor at a depth of 0.25 m. Figure 4 contains the complete time series of the principal stresses, σ_1 and σ_2, and the principal stress direction, θ, for this sensor. The convention used here is that compressive stresses are positive. The direction is relative to wire 1 in the sensor, which in this case was oriented towards the Polarbjorn. If the angle is positive, the direction is counterclockwise from the wire 1 orientation to the principal stress direction and if it is negative the angle is clockwise. The direction is referenced to the ship because it established a locally nonrotating frame of reference.

In general the stresses are at low levels, most often less than 50 kPa. There were only two time periods during which the stresses exceeded 100 kPa. The first of these occurred on days 312 and 313, during which lead formation, ridging and shear were observed locally. The drift direction of the ship and ice, normally in a southerly direction had turned northward during this period (Fig. 1). In addition, a warming trend began on day 311 and lasted until day 316, during which time the air temperature increased 17°C.

The other large stress event occurred on day 327 in the midst of the breakup of the ice in the local area as it approached Kvitoya (Fig. 1). Breakup began on day 321 when cracks formed in Alpha floe and continued to enlarge for the next several days. All floes in the local area began to disintegrate on day 325. By day 328 most floes in the area had been reduced in size to tens of meters, and nearly all of the first-year ice had been ridged, forcing the termination of the experiment. Multiyear ice was being heavily deformed and pushed into ridges during the extreme events. This sensor, which was located on a 100–200 m diameter remnant of Alpha recorded compressive stresses only slightly exceeding 125 kPa, relatively small stresses considering the amount of deformation taking place. Other sensors, to be discussed later, showed considerably larger stresses. It also appears that some tension was occurring during this period, very likely a result of the floe bending.

Prior to day 311, most of the stress changes observed were thermally induced, and are discussed in more detail in the following section. One exception noted was on day 294 when winds increased to 20 m s^{-1} and ridging was observed in newly frozen leads. The 60 kPa stresses observed at this time were at least partly due to mechanical activity as opposed to being completely thermally induced. The principal stress direction rotated counterclockwise 50° for this event indicating that the stress was oriented towards the near-edge of the floe (Fig. 2). A key difference between the thermally induced stresses and those due to ice deformation is that the thermal events occur over days while those due to deformation are higher frequency, occurring over tens of minutes or hours.

The principal components (σ_1 and σ_2) have very similar magnitudes until day 293. This implies that for the first part of the experiment when the stresses were small, they were generally isotropic. Later, when stresses increase as deformation increases, the stresses become anisotropic as would be expected. The principal stress directions indicate the same behavior. The directions are very noisy during low-stress periods. The direction became better defined

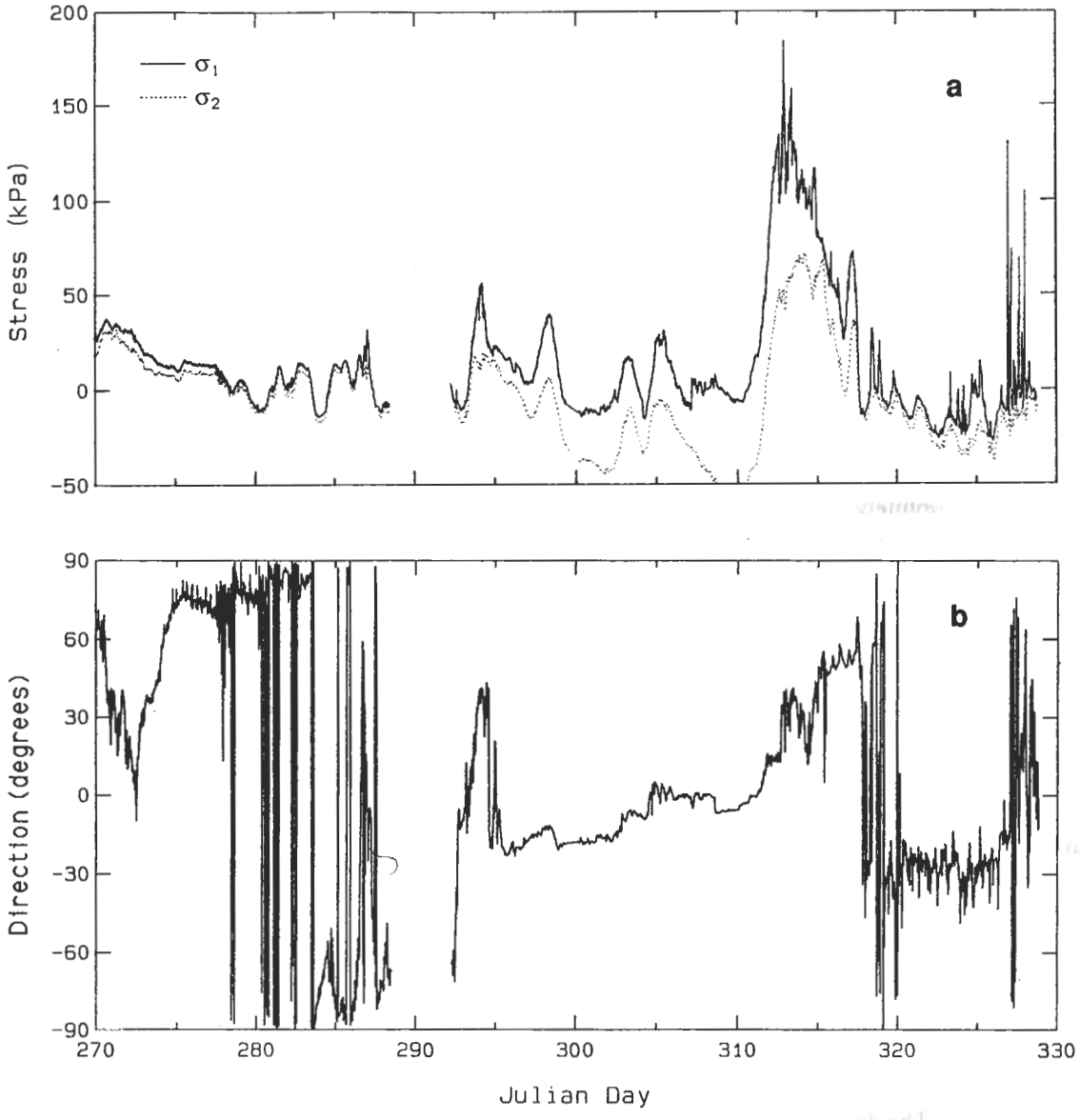

Fig. 4. Time series of principal stresses (a) and principal stress direction (b) from the 0.25 m sensor at site 1.

on day 295 when the magnitude of σ_1 and σ_2 began to differ.

Figure 5 contains the probability distribution of the σ_1 component for the time series. For the period, the mean stress was 14.4 kPa and the standard deviation was 29.0 kPa, with 70% of the stresses falling between −20 and +20 kPa. The most interesting characteristic of the histogram is that it is singularly peaked close to zero with a positive tail resulting from the larger compression events. It cannot be easily described by any common distribution. Tensile stresses are small but they are not uncommon. Compressive stresses reached 180 kPa only on day 313, when the thermal and dynamic stress events coincided. Stresses exceeding 100 kPa only occurred during the two large events mentioned and make up less than 4% of the measurements.

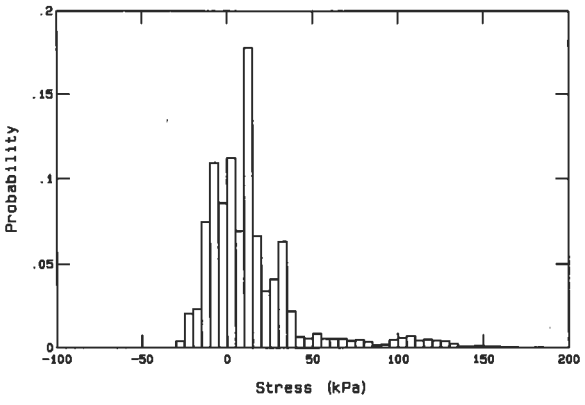

Fig. 5. Probability distribution of σ_1 stresses from the 0.25 m sensor at site 1 for the entire experiment.

Thermal stresses

Earlier researchers (Evans and Untersteiner, 1971; Bogorodsky et al., 1972; Milne, 1972; Cox, 1984) have established that significant stresses can be caused by rapid temperature changes in an ice sheet. Lewis and Denner (1988) and Lewis (1990) have proposed that thermally induced ice failure is responsible for much of the ambient noise observed in the Arctic Ocean. The large-stress event occurring between days 311 and 316 shown in Fig. 4 appears to have been thermally induced (with exception of the high-frequency event on days 312 and 313). In Fig. 6, temperature and stress data documenting this event in greater detail are presented. There was a significant warming trend (Fig. 6a) from day 311 to 313 as the air temperature increased from -32 to -15°C. The warming trend was also manifested in the ice temperatures. Data from the site 1 thermistor string are plotted in Fig. 6b. The temperature increase was limited to the upper half of the ice sheet and was quickest and most pronounced in the upper 0.20 m, with the ice temperatures warming 2 to 3°C by day 313.

In-situ ice stresses (σ_1) measured at site 1 in the top, middle and bottom of the floe are plotted in Fig. 6c. The change in stress was greatest for the top sensor, where the temperature changes were the largest. Stress variation at the top sensor was well correlated with the temperature record showing a rapid rise in compressive stress, followed by a gradual decline over the next several days. While the top of the floe was undergoing a large increasing compressive stress (~ 130 kPa), the middle and bottom sensors were reporting tensile stresses. Superposed over the thermal stresses was a brief increase in compressive stresses for all three sensors near day 313. As was mentioned earlier, this was associated with an overall convergence of the ice cover and included some small ridge-building events.

Thermally induced stresses can be understood by considering the expansion or contraction of an ice floe when it undergoes a temperature change. According to the theoretical work of Cox (1983) and the laboratory results of Johnson and Metzner (1990), the thermal expansion coefficient or sea ice is identical to that of fresh ice. Thus as sea ice warms it expands. This tendency towards expansion was greatest near the surface where the warming was largest. Since there was a structural connection vertically through the ice sheet, as the upper portion of the ice tried to expand the lower portion acted to retard this expansion, resulting in compression near the surface and tension below.

We can use a simple model developed by Bogorodsky et al. (1972) to examine this thermal stress event more quantitatively. They assumed an elastic ice rheology for an ice plate with free edges to derive an expression the vertical distribution of stress:

$$\sigma(z)=\frac{E(z)}{1-\nu}\left[\alpha\Delta T(z)-\frac{\int E(z)\alpha\Delta T(z)\mathrm{d}z}{\int E(z)\mathrm{d}z}\right] \qquad (1)$$

where the integrals are evaluated over the entire thickness of the ice, $\sigma(z)$ is the vertical distribution of stress, $\Delta T(z)$ is the temperature change with time at a given depth, α is the linear coefficient of thermal expansion (5×10^{-5}°C^{-1}), ν is Poisson's ratio (0.30) and $E(z)$ is the elastic modulus. Empirical modulus-brine volume relationships (Vaudrey, 1977; Tucker et al. 1989) were applied to the core data (Fig. 3) to determine the effective elastic modulus, $E(z)$. Changes in the ice temperature were calculated using data from a thermistor string located near the stress sensors.

Using this data, Eq. 1 was evaluated at depths corresponding to those of the stress sensors. There is general agreement between the observed and the calculated stresses (Fig. 6d) as they both show strong compression near the surface, and tension in the middle and bottom of the floe. There are, how-

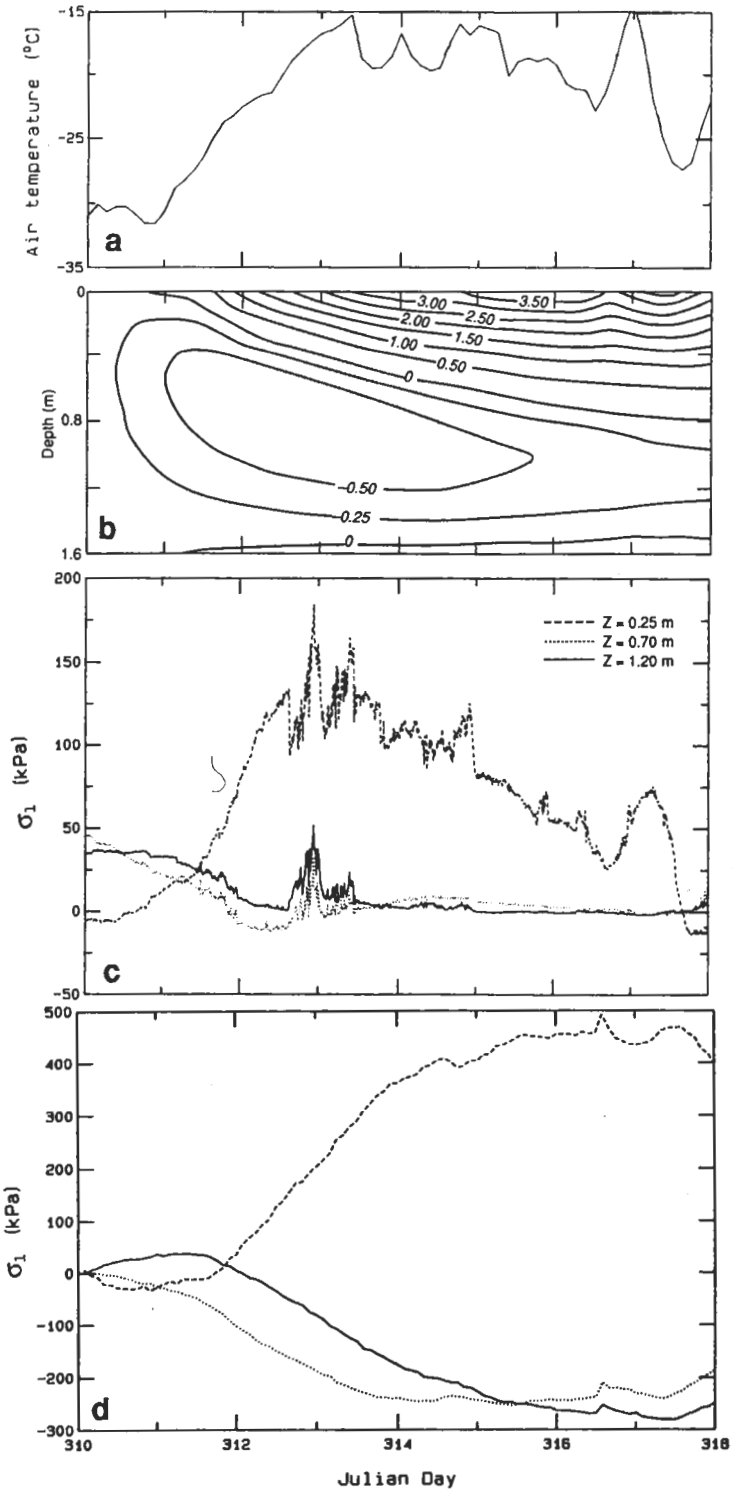

Fig. 6. Record of the thermal event at site 1. (a) Air temperature. (b) Contours of ice temperature (°C). (c) σ_1 stresses for the 0.25, 0.70, and 1.20 m deep sensors. (d) Model predictions of thermal stress for the observed ice temperatures.

ever, two major differences in the calculated values: (1) they are much larger than the observed values and (2) they do not decrease with time. Both these discrepancies are consistent with our failure to include ice creep in the model. The importance of creep was evidenced in the beginning of the experiment by the dissipation of the large freeze-in stresses over the course of a few days. The influence of creep is also apparent in the young ice record (Fig. 11), which because it is capable of more rapid creep, did not exhibit any evidence of thermal stress for this period. Lewis (1990) applied a more complex model which included a parameterization for the creep rate and obtained more reasonable agreement with this data.

In addition to this large event, other events were also thermally induced. A careful comparison of the ice temperatures and stress record for the top sensor at site 1 (Fig. 4) showed that virtually all of the stress changes of 20 to 50 kPa prior to day 310 were at least partly thermally induced, though warming or cooling was not as pronounced as that of day 311. Most of these smaller stress changes were associated with ice temperature changes of 0.5 to 0.8°C at the 0.25 m depth that occurred within a single day. Stress changes can be tensile or compressive, depending upon the sign of the temperature change. The important conclusion is that the thermal stresses are associated with rapid changes in ice temperature, on the time scale of a day or less. Creep nullifies stresses that would be produced by slowly varying temperatures.

Vertical variations

Vertical variations in stresses through the ice sheet can be assessed by examination of the data from site 1. We noted above for the thermally induced stresses, that the stress changes at mid-depth and deeper were of opposite sign and the magnitudes were significantly reduced from those in the upper layers of the ice. The question to be addressed here is whether the stresses associated with mechanical deformation are likewise reduced. Comfort and Ritch (1990) presented evidence that the stress magnitudes at mid-depth were about half of those observed in the upper quarter of the ice sheet.

Figure 6c shows evidence which agrees well with the findings of Comfort and Ritch (1990). While this figure is dominated by the thermal event discussed above, the mechanically caused event on day 313 was clearly documented by sensors at all depths. The stress increases for this event, independent of the thermal event are of interest. The magnitudes of the increases at the 0.7 and the 1.2 m depth are in very close agreement at about 50 kPa which was about 60% of the magnitude of the near-surface stress increase ($\sim$90 kPa).

Other major events that could be clearly associated with ice deformation occurred during the breakup period near the end of the experiment. Figure 7 shows the time series of the σ_1 components for the three depth levels for the most intensive 2 day period of the breakup. Here stresses have been further normalized such that the quiet periods were set to approximately zero stress for each sensor so the magnitudes could be easily compared. The figure indicates that large stresses were observed at all levels. For most events, the stresses near the bottom of the ice sheet are considerably less than those at higher levels. The stresses at mid-depth, however, are as large or larger than those at the shallow depth.

The probability distributions for the three sensors (Fig. 8) emphasize the differences in stresses at each level. The mean stresses at each level are 13.0, 22.7 and 6.8 kPa for the top, middle and bottom levels, respectively. Standard deviations were 23.1, 32.2 and 14.2 kPa. Clearly, lower stresses are exhibited by the deeper ice, where the largest stress observed was about 85 kPa. The largest stresses and the higher occurrences of large stresses were observed at mid-depth where the stress reached 150 kPa. The histograms show that the near-surface sensor was more likely than the middle sensor to have mean zero stress and the maximum stress reached only 130 kPa. Also fewer stresses exceeded 80 kPa than did at mid-depth.

The vertical distribution of stresses for the deformation events of day 313 and day 327 are substantially different. In one case, the stresses at depth are about half of those near the surface; in the other case stresses near the bottom of the sheet are about half of the surface values, but those at mid-depth are comparable to or larger than the surface. The only consistent relationship is that the stresses near the

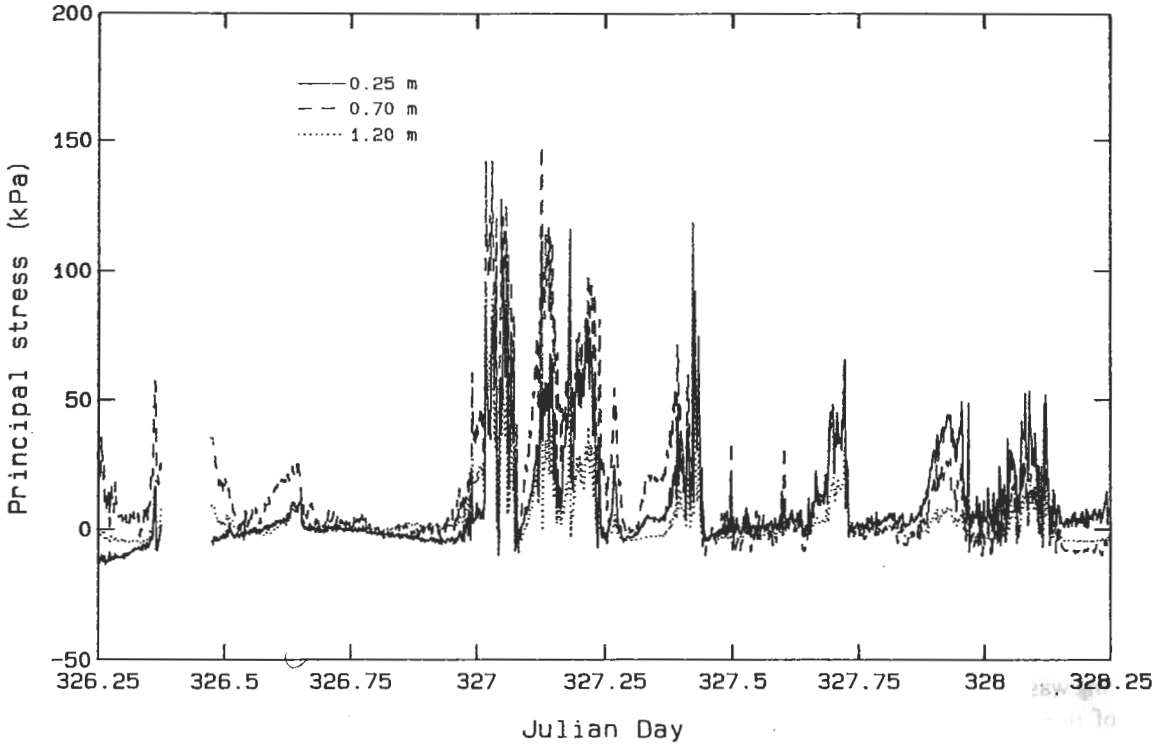

Fig. 7. Principal stresses (σ_1) during breakup for the 0.25, 0.70 and 1.20 m deep sensors at site 1.

bottom of the ice are about half those at the shallow depth.

We can examine a simple example of in-plane forcing to shed light on the vertical stress distribution. For the first-order approximation, we assume homogeneity and linear-elastic ice behavior. A multiyear floe of thickness h has a horizontal force F placed on it by adjacent first-year ice of thickness h'. The eccentric load results in the force and a moment M acting about the centroid of the multiyear floe. Simple static beam theory shows that the vertical stresses vary with distance z away from the neutral axis as:

$$\sigma(z)=\frac{F}{h}+\frac{6F(h-h')z}{h^3} \qquad (2)$$

where the second term is due to the bending moment which will be positive (compression) above the neutral axis and negative below the neutral axis. Thus the bending moment acts to increase the compressive stress above mid-depth and decrease it below, with possibly tension near the bottom of the sheet.

If we assume that floe Alpha was subjected to in-plane forcing from 0.5 m thick first-year ice, Eq. 2 predicts that the stresses at the 0.7 m deep sensor should be 51% of those observed by the 0.25 m deep sensor. This is in reasonable agreement with the dynamic stresses observed on day 313. Stresses at the 1.2 m depth should be about zero, however. The model also does not account for the vertical distribution observed on day 327. While this simple model demonstrates that a simple vertical distribution of stresses might be expected in an ideal case, the data indicate that the situation is far more complex than we have represented. For instance, the ice will not behave elastically under sustained loading, and ice properties and thickness are certainly not homogeneous.

We can only speculate as to the causes of the differences in the vertical distribution of stresses between the events on day 313 and 327. On day 313 a considerable amount of first-year ice existed in the

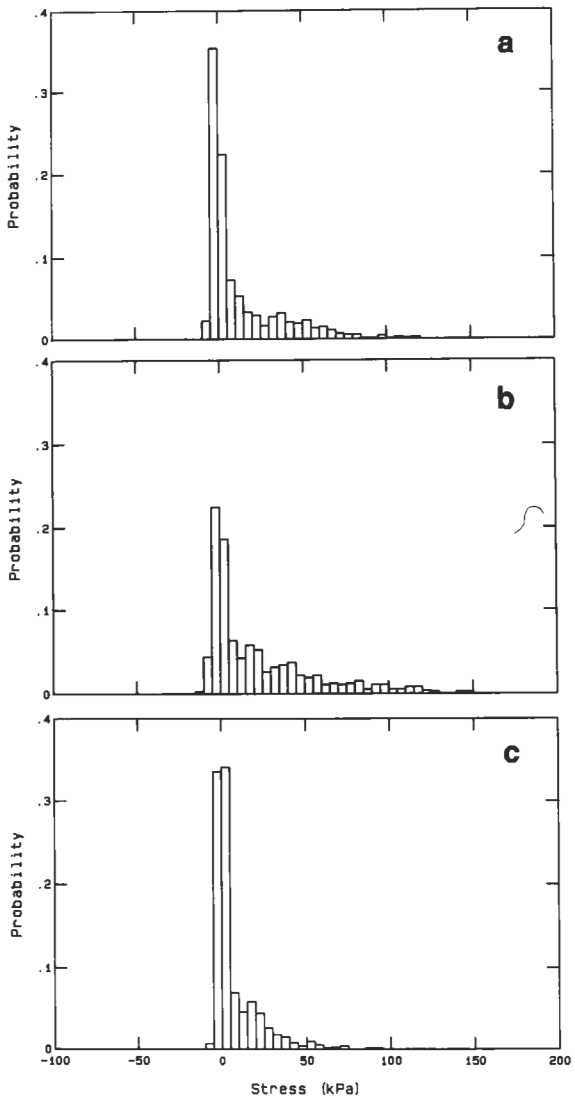

Fig. 8. Probability distributions for the breakup event shown in Fig. 7 for the (a) 0.25 m, (b) 0.70 m and (c) 1.20 m deep sensors at site 1.

area. The small convergence noted in the strain data on this day (Tucker et al., 1991) resulted in some local ridge building. We might then assume that the floe was loaded across a wide front by a thin ice sheet (0.2–0.5 m), presenting a loading scenario as described above, only complicated by inelastic behavior and variable ice properties. On day 327, observations confirmed that most of the first-year ice in the area had been ridged. During this time the multiyear ice was being ridged and sheared. Thus while contact areas may have been across wide fronts, the loads would likely have been distributed over greater ice thicknesses since the floe was probably in direct contact with other multiyear floes or ridges. In this case, larger stresses would have been distributed through more of the ice thickness. It is difficult to imagine a loading situation that produces the largest stresses at mid-depth, except one in which the major contact points are at some depth within the ice.

Clearly, the vertical distribution of stresses changed from one event to the other. Thus if the objective is to measure pack ice forces, it is necessary to monitor stress at more than one depth. This enables the average stress through the ice thickness to be accurately determined. If we assume that the ice sheet is composed of three levels of equal thickness with uniform stresses within each level corresponding to those which we observed, we can calculate average stresses. The average stress for the dynamic event on day 313 was about 63 kPa and that for the largest stresses on day 327 was 118 kPa. These average stresses correspond to forces per unit width for 1.6 m ice of 100 and 190 kN m^{-1}. If the stresses observed by the shallow sensor alone had been taken as the average stress for these two events the calculated forces would have been 144 and 210 kN m^{-1}, somewhat larger than estimates made using the more realistic average stresses.

Horizontal variations

Another objective of this program was to examine the spatial variations in ice stresses that are observed in an ice floe or between floes. This problem has been somewhat addressed by Croasdale et al. (1988) and Comfort and Ritch (1990), however the results were obscured by the fact that different types of sensors were used. Our own results are also somewhat limited since our investigation of horizontal variations in ice stresses consisted only of three near-surface sensors on two different floes.

In Fig. 9, the time series of σ_1 components for the more dynamically active part of the experiment, days 310–328, are shown for the three shallow sensors. These include sensor a at site 1, and sensors b and c from site 2. Sensor a was located about 200 m from the edge of floe Alpha while sensors b and c

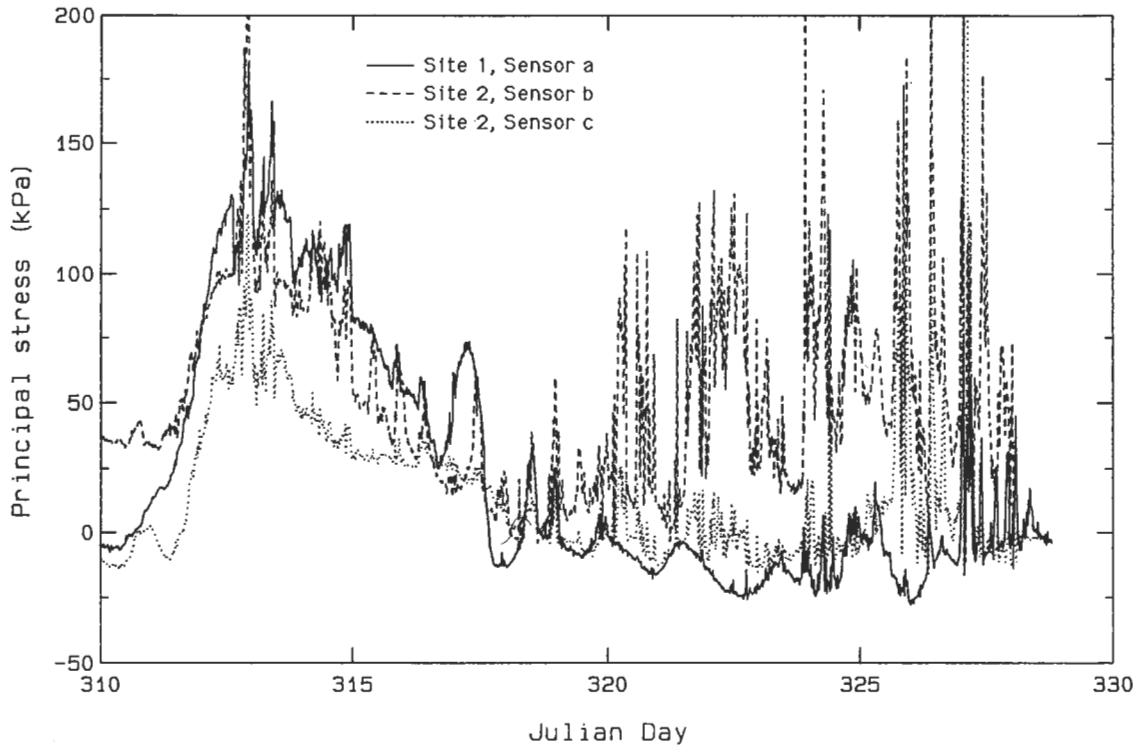

Fig. 9. Principal stresses (σ_1) for site 1 sensor a, and b, and c of site 2 for days 310–328.

were 2 and 15 m, respectively, from the edge of Beta floe abutting a frozen lead (Fig. 2). Principal stress directions are now shown, but it is worth noting that the directions between the sensors b and c were in reasonable agreement and they were much more variable than those for sensor a on Alpha whose principal direction is shown in Fig. 4. The only reasonable agreement between stresses at the three locations was for the long-term thermally induced stress event from day 311 to day 316, which is well characterized on all records. The stress increase attributable to the thermal event alone was about 125 kPa on floe Alpha and 60–70 kPa at the two sensor locations on Beta. The stresses associated with the high-frequency deformation event of day 313 superposed on the thermal event are also similar. All records show increases of 75 to 100 kPa.

The similarity between the three stress records appears to end with the thermal event. Beginning on day 320 the near-edge sensor (b) on Beta indicates a continuing series of large-stress events for the remainder of the experiment. Sensor c, located only 13 m away, also indicated high-frequency events associated with dynamic activity beginning at this same time which generally coincided with those at b. The magnitudes of the stress changes were generally far less than those near the floe boundary, however. The dynamic events were not apparent at site 1 on Alpha floe until day 324. The increased activity leading to breakup was certainly best characterized by the record of sensor b, where stresses exceeding 100 kPa were frequently observed.

The probability distributions (Fig. 10) further illustrate the differences between sites. The stresses on Alpha (Fig. 10a) cover a large range, from small tensile to compressive stresses as large as 180 kPa. For this period, the mean stress was 24 kPa, and 56% of the stresses fell between -20 and $+20$ kPa. The most dramatic stresses are exhibited by the near-edge location b, on Beta (Fig. 10b), where the mean stress for the period was 53 kPa. It also experienced the greatest percentages of large stresses, particularly in the 30 to 120 kPa range with only 20% of the stresses in the range -20 to $+20$ kPa.

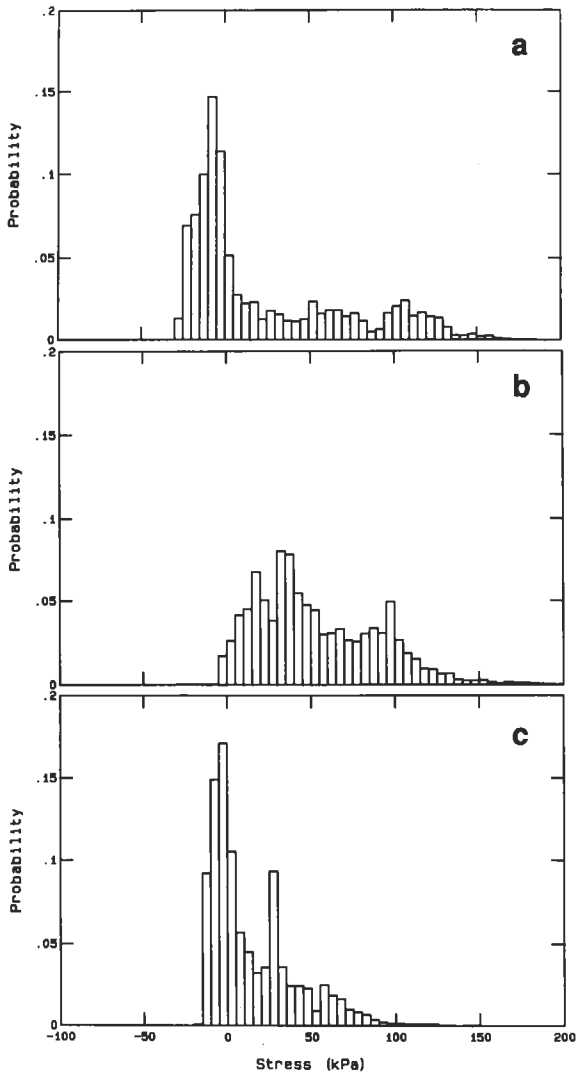

Fig. 10. Probability distributions for (a) site 1 sensor a, and (b) sensor b, and (c) sensor c of site 2 for days 310–328.

On the other hand, the near-surface stresses recorded by sensor c (Fig. 10c) are significantly less than at either of the other locations, 60% lying between −20 and +20 kPa. Stresses larger than 200 kPa, which are not shown on the histograms, occurred at site 2 during the breakup period. Only very small tensile stresses were observed at either Beta location. The thermal event was responsible for most of the larger stresses observed by sensor a on Alpha. A regression analysis between the stresses observed at b and c on Beta showed that the stresses were not particularly well correlated, with a cross correlation coefficient between the two stress records of 0.53.

The discrepancies in the stresses between these three locations are not unexpected. The obvious indication is that stress activity is significantly higher near the edge of the floe and that this activity is rapidly diminished away from the edge. This is in general agreement with the numerical modeling results of Frederking and Evgin (1990) who examined cases of loads applied over limited widths. It is apparent here, however, that there is no simple relationship between stresses observed at near or far locations. The large differences in stresses between the closely located sites on Beta are due to a number of factors. Most important is the type of interaction occurring between the multiyear ice near the boundary of the floe and the first-year ice. The location of sensor b near the edge was apparently a very active contact point subsequent to day 320. The magnitudes of the stresses were rapidly attenuated away from the edge. The degree of attenuation no doubt depends upon the variability of ice properties and thickness, the direction of loading, the geometry of the floe relative to the contact area, and the bending moments established. The stresses at the Alpha location were further diminished relative to the more frequent dynamic activity near the floe boundary, thus may tend to be more representative of average pack ice conditions.

Young vs. multiyear ice

It has been mentioned previously that the sensor in first-year ice showed neither the residual stresses nor the long-term drift that was evident in the records of multiyear sensors. A more detailed comparison between the stresses observed in the first-year ice to those in the adjacent multiyear ice is now presented. Figure 11 contains the day 310 to day 328 σ_1 record of sensors a and b at site 2, where sensor a was 0.2 m deep in 0.4–0.5 m thick first-year ice and sensor b was located at a depth of 0.25 m in 2.0 m multiyear ice. Sensor a was 7.0 m out into the first-year ice while b was 2 m from the edge of the multiyear floe. The most striking feature of Fig. 11 is that the high-frequency events from both locations are well correlated, but the low-frequency thermal

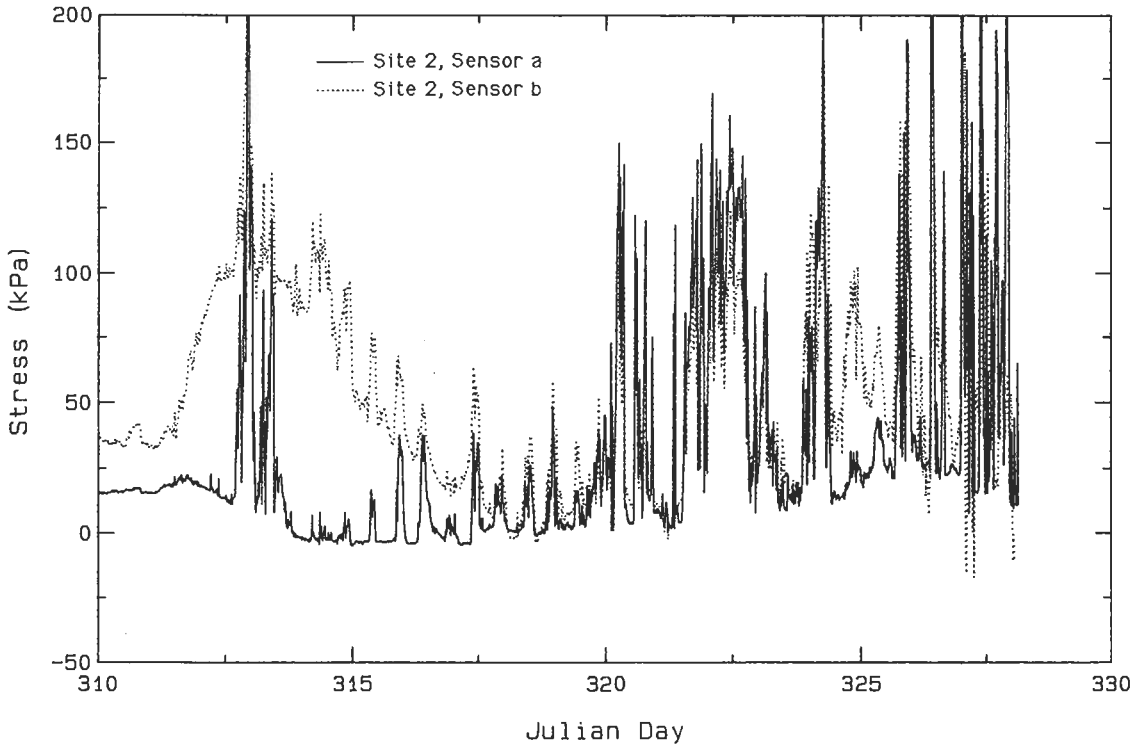

Fig. 11. Principal stresses (σ_1) for sensors a and b of site 2. Sensor a was located in the first-year ice and b was in the adjacent multiyear ice 2.0 m from the edge of the floe.

event of days 312 to 316 is not at all evident in the first-year ice stresses. The dynamic event occurring on day 313 which is superposed on the thermal stress in the multiyear record is very obvious in the first-year ice record. Also, stress oscillations which appear to have a repetition rate of about twice daily are clear in both sensor records beginning on day 314 and lasting until the initiation of breakup on day 321.

Figure 12 contains the σ_1 components of stress for the first-year ice plotted against those of the multiyear ice for days 317 to 328, allowing a better contrast of the dynamic events alone. The stresses between these two locations agree surprisingly well. A cross correlation between the two records yielded a coefficient of 0.75. Even higher correlation between the stresses occurred between days 320 and 324, when a coefficient of 0.98 was obtained. This exceptionally well correlated period is that portion of Fig. 12 for which the stresses are in nearly linear agreement. A linear regression of the stresses occurring between days 320–324 indicated that the magnitudes of the near-edge multiyear stresses were 70% of the young ice values. For the same period, stresses from sensor c, 15 m from the edge of the floe, produced a coefficient of 0.82 when correlated with the first-year record. While the high coefficient indicates that events were reasonably in phase, a regression showed that the magnitudes of the stresses were only 17% of the first-year values. The close coupling between the first-year ice and the near-edge multiyear ice is emphasized here, as is the rapid attenuation of that coupling as distance from the edge is increased.

Breakup stresses

The events occurring during the intense breakup period warrant attention because they contain the largest stresses observed on the experiment. The records from site 2 are especially interesting because ice failures occurred very near the sensors.

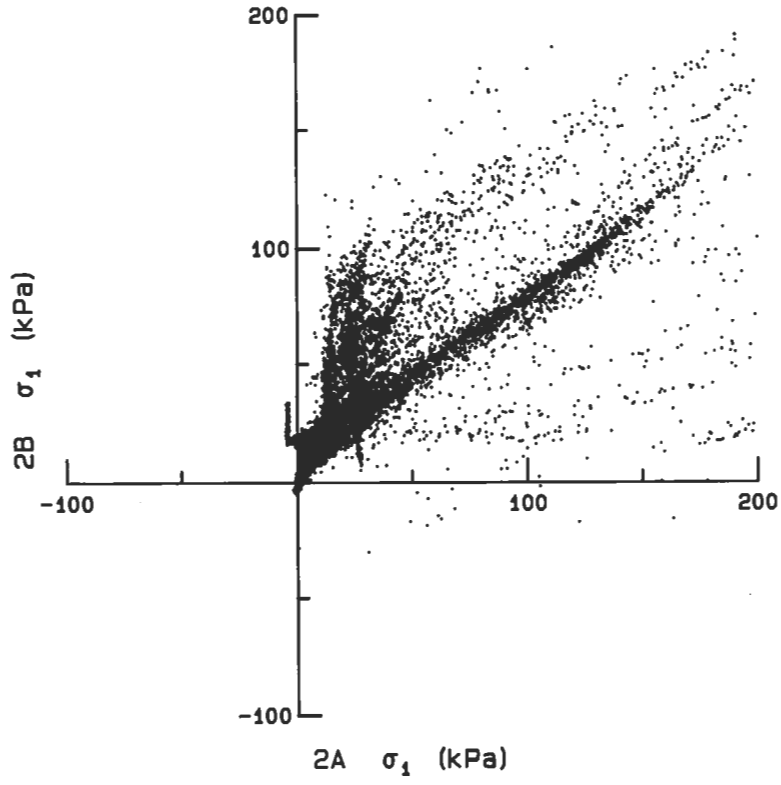

Fig. 12. Scatter plot of principal stresses (σ_1) for sensors a and b of site 2 for days 317–328.

This was visually ascertained during recovery of this system on day 328. At that time, the data-logging system and one of the sensors were located on a freely floating 5 m diameter multiyear chunk; the other two sensors had been severed from the system.

Figure 13 shows an expanded time series plot of the σ_1 components for the last two days that the sensors at site 2 were operable. For the events of day 326, the records from the sensors in first-year ice (a), and both sensors in multiyear ice (b and c) were well correlated. The magnitudes were as described previously, with the largest stresses in the first-year ice, then diminishing away from the edge of the multiyear floe. During the one large event on day 326, maximum stresses for sensors a and b were 440 and 260 kPa, the largest stresses recorded by these sensors during the experiment.

On day 327, the behavior of the three sensors changed character. During the large event early on day 327, the stress events observed by the sensors are out of phase. A maximum stress of 460 kPa was recorded by sensor c, the largest stress recorded during the experiment by any sensor. This sensor, 15 m from the edge of the floe, had previously shown greatly reduced stresses. Following this event, stresses observed by sensor c for the remainder of the experiment were negligible. Significant stresses continued to occur in the first-year and near-edge multiyear ice until cable separation early on day 328, although the magnitudes of the stresses are different and they appear to be out of phase for some events. This most likely indicates a loss of coupling between the multiyear and first-year ice. We suspect that both the multiyear and first-year ice sheets experienced significant failures during the event on day 327.

The stresses observed during breakup at site 1 (Fig. 7) were substantially different. This site remained intact on a surviving 100–200 m diameter remnant of the large Alpha floe. The largest stresses recorded by the near-surface sensor were 130 kPa while at mid-depth they reached 150 kPa. The dif-

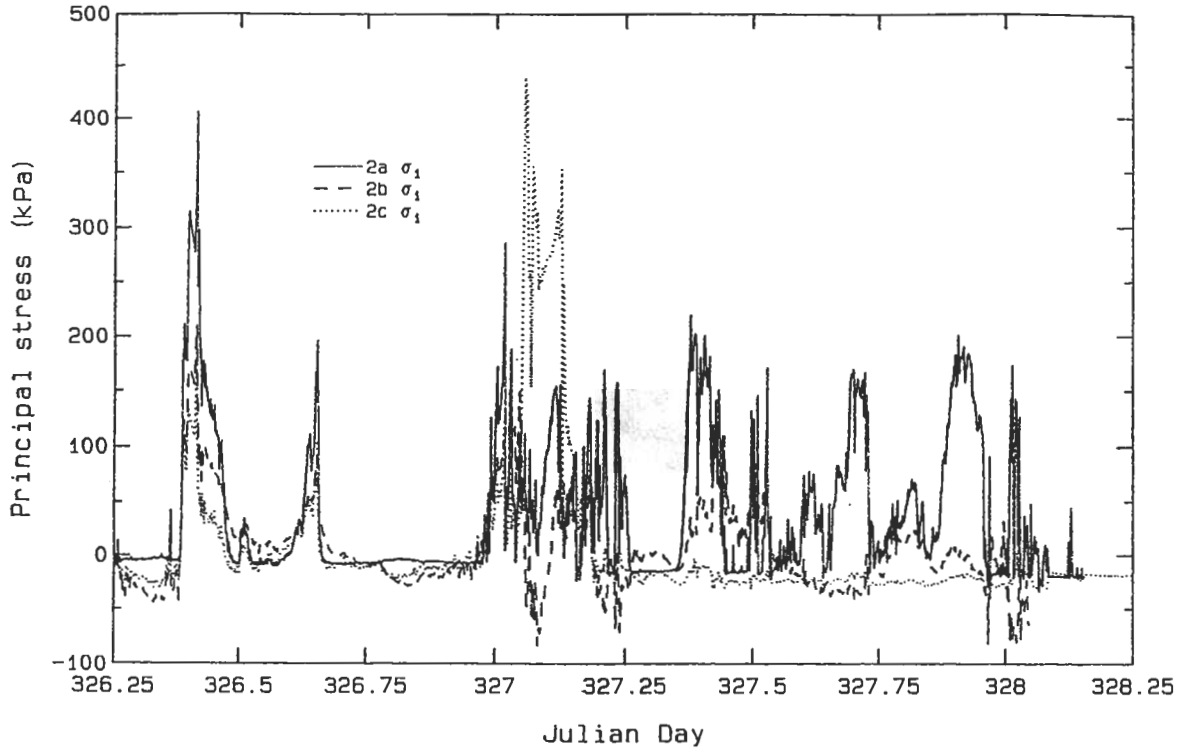

Fig. 13. Principal stresses (σ_1) for sensors a, b and c of site 2 during breakup.

ferences in stresses observed at the two sites were related to their proximities to ice failures. At site 2, the sensors were undoubtably very near local failures. That the stress events of the three sensors fell out of phase indicates decoupling of the once intact ice sheets, possibly occurring during nonsimultaneous and mixed-mode failures. At site 1, stresses were significantly less because they have been attenuated with distance from the failure locations. This site would be more representative of average stresses during breakup, while site 2 experienced stresses associated with point source local failures.

Oscillations

Periodic oscillations are evident in the stress records of site 2 sensors a and b following day 314 (Fig. 11). Qualitatively, these oscillations were apparent to the field party as a twice daily grinding and listing of the ship. More quantitatively, they appeared in a number of the drift phase data sets including measurements of stress, acceleration and ambient noise (Pritchard, 1990). Oscillations in stress were clearest in the young ice record (Fig. 14) which showed regular increases in stress with magnitudes of 25–50 kPa between day 314 and day 320. A power spectrum (Fig. 14, insert) of the stress time series was computed after removing the mean, zero-padding and applying a Welch filter. The oscillations appear as a distinct spike in the power spectrum with a period between 11.9 and 12.4 hours.

These oscillations could possibly be the result of inertial effects. McPhee (1977) examined the role of inertial oscillations in the Beaufort Sea ice pack. He pointed out that inertial oscillations are most likely to occur when the internal ice stress is small, such as in summer and early fall, and that they are initiated by sudden shifts in the wind. At a latitude of 81°N the inertial oscillation period is 12.2 hours per cycle, which lies in the middle of the peak of the stress power spectrum. However, it is difficult to rule out the influence of tides. In fact the principal lunar tide component (M2) has a period of 12.4 hours, equal to the peak period of the stress data. The drift

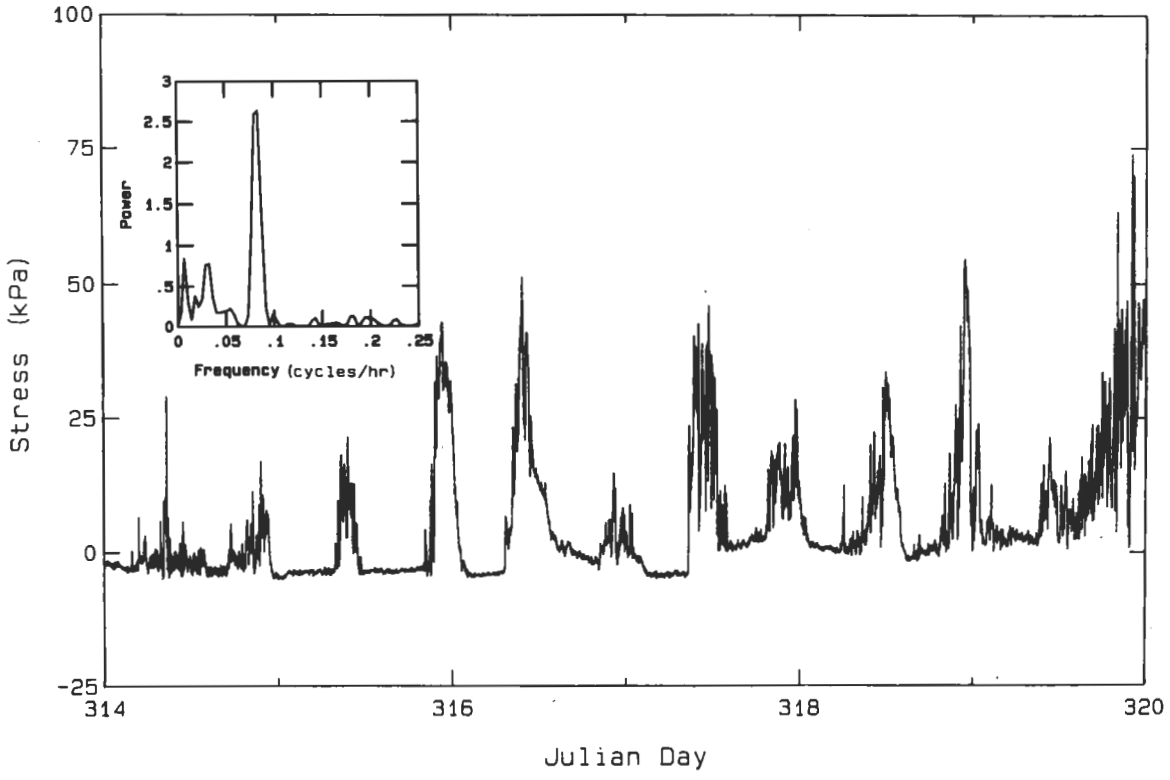

Fig. 14. Principal stresses (σ_1) of the first-year ice sensor at site 2 (a) for days 314–320. Power spectrum of the time series is shown as an insert.

track of the ship (Fig. 4c; McPhee, 1990) is also ambiguous in that it shows the distinctly cycloidal motion associated with inertial oscillations, but it also shows that the oscillations began as the floe entered shallow water where tidal effects would increase. In fact, it is possible that both an inertial and tidal component are contained in the stress data. Additional information is needed to conclusively distinguish between these two mechanisms.

The oscillations were only clearly evident in the stress records of sensors a and b of site 2. It appears that this signal was most prevalent in the first-year ice and the strong interaction between the first-year ice and the near-edge multiyear ice resulted in it being obvious at the location of sensor b. It is likely that the force associated with the oscillation is large enough to cause a detectable stress in the first-year ice but induced stresses are rapidly attenuated in the thicker multiyear ice.

Conclusions

The two months of stress measurements obtained in the eastern Arctic have produced some surprising and enlightening results regarding *in-situ* ice stresses. There was an element of serendipity in that the measurements were obtained during a period when radical weather variations caused large temperature changes and dynamic activity stimulated large-deformation events.

Most surprising were the thermally induced stresses. The largest thermal stress observed was a compressive stress increase of about 130 kPa in the near-surface layer accompanied by small tensile stresses at depth. This event was associated with an air temperature increase of 17°C over two days which caused the ice temperature to warm 2–3°C at a depth of 0.25 m. Other smaller thermal stresses were observed at the shallow sensor location on Al-

pha floe which were triggered by ice temperature changes of at least 0.5°C day^{-1}.

The vertical distribution of stresses varied considerably during dynamic events. At the deeper location near the bottom of the ice sheet, stresses were about half those of the surface values. At mid-depth, no such convenient relationship was apparent. During one event mid-depth stresses were about 60% of those occurring at the surface, yet during the major break-up, they were slightly larger than the surface values.

Significant horizontal variability of stress over short distances was observed. At a site near the edge of a multiyear floe, dynamically induced stresses were observed that were well correlated with those in the adjacent thin first-year ice. However, they were poorly correlated with stresses in the same ice floe only 13 m away. Stresses observed at a site 200 m from the floe boundary on an adjacent floe had much reduced levels over those near the edge. It appears that stresses observed at this site may have been more representative of average pack ice forces. Clearly, more observations of spatial stress variations are necessary in addition to detailed numerical modeling where the anisotropy of ice properties can be taken into account.

The stresses recorded at the first-year ice site were generally larger and more frequent than the other sites. There was a high degree of coupling between the first-year ice and the adjacent multiyear site. Both sites also exhibited stresses of about 50 kPa at 12 hour intervals which were probably associated with tidal or inertial oscillations of the ice sheet. Other multiyear ice sites showed little or no evidence of these oscillations. The first-year ice site did not exhibit the thermal stresses seen by all near-surface multiyear sensors.

The largest stresses were observed during breakup by the sensors located in first-year and multiyear ice at site 2. Stress magnitudes exceeded 400 kPa in both types of ice during single instances of local ice failure. For the near-surface site on Alpha the stress increases during breakup only reached 130 kPa while at a depth of 0.7 m they were 150 and 80 kPa at 1.20 m. Distance from the failure zones attenuated the stresses associated with local failures. The largest stresses observed at site 1 were generated by a combination of the thermal and dynamic events, which produced a surface stress of about 180 kPa. Tensile stresses were largest at the shallow sensor of the Alpha site, where they reached 30 kPa.

It is not surprising that the largest stresses were observed at the near-edge sites where active deformation and failure occurred. The large stresses observed here resulted from the close proximity of local deformation events. That stresses observed at site 1 were significantly less lends support to the hypothesis that it will be necessary to place instruments far from the edge of the floe to adequately observe spatially averaged pack ice pressures. The preferable location is the center of a large floe where the zone of influence is much larger, and stresses will reflect average pressures resulting from large-scale events.

Laboratory tests indicate compressive strengths of small-scale ($\sim$0.1 m) ice samples (depending upon confinement, strain rate and temperature) ranging from 1 to 10 MPa. In large-scale ice dynamics models ($\sim$50–100 km) it is necessary to limit geophysical scale ice strengths to 5 to 50 kPa to obtain reasonable results. Our observations fall comfortably between these two extremes which bridge four orders of magnitude. Our estimates of ridge-building forces of 100–200 kN m^{-1} also fall well within the estimates spanning several orders of magnitude assembled by Croasdale (1984).

Acknowledgements

The authors gratefully acknowledge the support of the Arctic Program, Office of Naval Research who made it possible for us to conduct these measurements on the CEAREX program. This work was funded under contracts N0001489WM24004 and N0001490MP24051.

References

Bogorodsky, V.V., Gavrilo, V.P., Gusev, A.V., Gudkovich, Z.M. and Polyakov, A.P., 1972. Stressed ice cover state due to thermal wave and related underwater noise in the ocean. Proc. Ice Symposium 1972, Leningrad. AIRH Translation, pp. 28–33.

Comfort, G. and Ritch, R., 1989. Field measurements of pack ice stresses, Vol. 1—Main Report. Fleet Technology, Ltd. report prepared for Public Works Canada. 129 pp.

Comfort, G. and Ritch, R., 1990. Field measurement of pack ice stresses. Proc. 9th Int. Conf. of Offshore Mechanics and Arctic Engineering, Houston, ASME Book 10296F, pp. 177–181.

Coon, M.D., Lau, P.A., Bailey, S.H. and Taylor, B.J., 1989. Observations of ice floe stress in the eastern Arctic. In: K.B.E. Axelsson and L.A. Fransson (Editors), Proc. 10th Int. Conf. on Port and Ocean Engineering under Arctic conditions, Lulea, Sweden, POAC-89, Vol. 1: 1943–1973.

Cox, G.F.N., 1983. Thermal expansion of saline ice. J. of Glaciol., 29(103): 425–432.

Cox, G.F.N., 1984. A preliminary investigation of thermal ice pressures. Cold Reg. Sci. Technol., 9: 221–229.

Cox, G.F.N. and Johnson, J.B., 1983. Stress measurements in ice. U.S. Army Corps Eng. Cold Reg. Res. Eng. Lab. Rep. 83–23, 31 pp.

Cox, G.F.N. and Weeks, W.F., 1983. Equations for determining the gas and brine volumes in sea ice. J. Glaciol., 12: 309–316.

Croasdale, K.R., 1984. The limiting driving force approach to ice loads. Proc. of Offshore Technology Conference 1984, OTC Pap., 4716: 57–64.

Croasdale, K.R., Comfort, G., Frederking, R., Graham, B.W. and Lewis, E.L., 1988. A pilot experiment to measure Arctic pack ice driving forces. In: W.M. Sackinger and M.O. Jefferies (Editors), Port and Ocean Engineering under Arctic Conditions. Univ. of Alaska, Vol. III, pp. 381–395.

Evans, R.J. and Untersteiner, N., 1971. Thermal cracks in floating ice sheets. J. Geophys. Res., 76(3): 694–703.

Frederking, R.M.W. and Evgin, E., 1990. Analysis of stress distributions in an ice floe. Proc. 9th Int. Conf. of Offshore Mechanics and Arctic Engineering, ASME Book 10296F, pp. 83–87.

Graham, B.W., Chabot, L.G. and Pilkington, B.R., 1983. Ice load sensors for offshore Arctic structures. Proc. 7th Int. Conf. on Port and Ocean Engineering under Arctic Conditions, Helsinki, 4: 547–562.

Hawkins, J.R., James, D.A. and Der, C.Y., 1983. Design, construction and installation of a system to measure environmental forces on a caisson retained island. Proc. 7th Int. Conf. on Port and Ocean Engineering under Arctic Conditions, Helsinki, Vol. 4: 770–779.

Hibler, W.D. III, 1980. Modeling a variable thickness sea ice cover. Mon. Weather Rev., 108(12): 1943–1973.

Johnson, J.B., Cox, G.F.N. and Tucker, W.B. III, 1985. Kadluk ice stress measurement program. Proc. 8th Int. Conf. on Port and Ocean Engineering under Arctic Conditions, Narssarssuaq, Greenland, Vol. 1: 88–100.

Johnson, J.B. and Metzner, R., 1990. Thermal expansion of saline ice. J. Glaciol., 36(124): 343–349.

Lewis, J.K., 1990. Generation mechanisms for lower and higher frequency Arctic ambient noise. Science Applications International Corporation, Rep. SAIC-90/1449, 15 pp.

Lewis, J.K. and Denner, W.W., 1988. Higher frequency ambient noise in the Arctic Ocean. J. Acoust. Soc. Am., 84: 1444–1455.

McPhee, M.G., 1977. A simulation of inertial oscillations observed in the drift of manned stations. AIDJEX Bull., 36: 65–86.

McPhee, M.G., 1990. CEAREX 1988 Polarbjorn drift: position and velocity analysis. McPhee Research Company, Tech. Rep., 34 pp.

Milne, A.R., 1972. Thermal tension cracking in sea ice: a source of underice noise. J. Geophys. Res., 77: 2177–2192.

Pritchard, R.S., 1990. CEAREX drift experiment. EOS, 71(4): 1115–1118.

Rothrock, D.A., 1975. The energetics of plastic deformation of pack ice by ridging. J. Geophys. Res., 80: 4514–4519.

Tucker, W.B. III, Richter-Menge, J.A. and Gow, A.J., 1989. Variations in mechanical properties within a multiyear ice floe. Proc. of Oceans '89, Seattle, pp. 1287–1291.

Tucker, W.B., Perovich, D.K., Hopkins, M.A. and Hibler, W.D., III, 1991. On the relationship between local stresses and strains in Arctic pack ice. Ann. Glaciol., In Press.

Vaudrey, K.D., 1977. Ice engineering: Study of related properties of floating sea-ice sheets and summary of elastic and viscoelastic analysis. Naval Civil Engineering Laboratory, Port Hueneme, Calif., Rep. TR-860, 181 pp.

Vivatrat, V. and Kreider, J.R., 1981. Ice force prediction using a limited driving force approach. Proc. of Offshore Technology Conference, OTC, P. 4115: 471–485.